Polymerization Hot Paper

How to cite:
International Edition: doi.org/10.1002/anie.202010696
German Edition: doi.org/10.1002/ange.202010696

Metallo-Helicoid with Double Rims: Polymerization Followed by Folding by Intramolecular Coordination

*Guang-Qiang Yin, Sneha Kandapal, Chung-Hao Liu, Heng Wang, Jianxiang Huang, Shu-Ting Jiang, Tan Ji, Yu Yan, Sandra Khalife, Ruhong Zhou, Libin Ye, Bingqian Xu, Hai-Bo Yang, Mu-Ping Nieh, and Xiaopeng Li**

Abstract: *In this study, we established a feasible strategy to construct a new type of metallo-polymer with helicoidal structure through the combination of covalent polymerization and intramolecular coordination-driven self-assembly. In the design, a tetratopic monomer (**M**) was prepared with two terminal alkynes in the outer rim for polymerization, and two terpyridines (TPYs) in the inner rim for subsequent folding by selective intramolecular coordination. Then, the linear covalent polymer (**P**) was synthesized by polymerization of **M** via Glaser-Hay homocoupling reaction. Finally, intramolecular coordination interactions between TPYs and Zn(II) folded the backbone of **P** into a right- or left-handed metallo-helicoid (**H**) with double rims. Owing to multiple positive charges on the inner rim of helicoid, double-stranded DNA molecules (dsDNA) could interact with **H** through electrostatic interactions. Remarkably, dsDNA allowed exclusive formation of **H** with right handedness by means of chiral induction.*

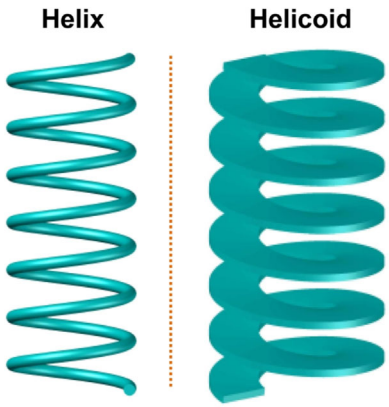

Figure 1. Cartoon representation of helix (left) and helicoid (right).

Introduction

In geometry, helicoid is the third minimal surface to be known, after the plane and catenoid.[1] As the name derived from its similarity to the helix, helicoidal structure consists of numerous parallel-arranged helices as its boundary (Figure 1). As one type of topological structure with inherent chirality, helical structures are ubiquitous in nature.[2] Helical or spiral biopolymers play prominent roles in sophisticated biological processes such as genetic encoding, chiral catalysis as well as self-assembly of cellular components.[3] To mimic the complexity and functionality of helical biopolymers in nature, a variety of artificial helical oligomers and polymers have been successfully constructed with the aid of reversible non-covalent forces, i.e., metal-coordination interactions,[4] hydrogen bonding,[5] electrostatic attraction,[6] and π-π interactions.[7] Compared to the flourish of helical polymers, the spiral polymers with helicoidal structures still remain less explored, perhaps because of the challenge of design and synthesis of multi-rimmed or multi-layered monomer to afford parallel-arranged helix as the boundary helicoidal polymers in a well-controlled manner.

Among the artificial helical polymers, acetylene-based helical polymers have been widely studied on account of their facile synthesis, handleability, the host ability of tubular

[*] Dr. G.-Q. Yin, Dr. H. Wang, Dr. X. Li
College of Chemistry and Environmental Engineering, Shenzhen University
Shenzhen, Guangdong 518055 (China)
E-mail: xiaopengli@szu.edu.cn

S. Kandapal, Dr. B. Xu
Single Molecule Study Laboratory, College of Engineering and Nanoscale Science and Engineering Center, University of Georgia
Athens, GA 30602 (USA)

C.-H. Liu, Dr. M.-P. Nieh
Department of Chemical and Biomolecular Engineering, University of Connecticut
Storrs, CT 06269 (USA)

S.-T. Jiang, T. Ji, Dr. H.-B. Yang
Shanghai Key Laboratory of Green Chemistry and Chemical Processes, Department of Chemistry, East China Normal University
Shanghai 200062 (China)

Y. Yan, S. Khalife
Department of Chemistry, University of South Florida
Tampa, FL 33620 (USA)

Dr. L. Ye
Department of Cell Biology, Microbiology and Molecular Biology, University of South Florida
Tampa, FL 33620 (USA)

Dr. M.-P. Nieh
Polymer Program, Institute of Material Science, University of Connecticut
Storrs, CT 06269 (USA)

Dr. J. Huang, Dr. R. Zhou
Institute of Quantitative Biology, Zhejiang University
Hangzhou, Zhejiang, 310027 (China)

Supporting information and the ORCID identification number(s) for the author(s) of this article can be found under: https://doi.org/10.1002/anie.202010696.

cavity, and structural diversity.[8] However, the spiral conformation of most of the reported acetylene-based helical polymers with single chain (or rim) of backbone was sensitive to the solvents and temperature due to the weak interactions. In the past few years, 2,2′:6′,2″-terpyridine (TPY) has been broadly utilized to construct various metallo-polymers owing to its versatile binding affinity towards transition metal ions.[9] In TPY-based metallo-polymers, TPYs could be introduced into conventional polymers as pendant groups for further coordination, or act as the terminal chelation moieties for supramolecular polymerization.[9a,d,10] The systems with multiple TPYs as pendant groups generally experienced both intermolecular and intramolecular coordination without precise control; While monomers with two terminal TPYs were polymerized by intermolecular coordination to form metallo-supramolecular polymers with labile main chains.

To tackle the challenge of helicoidal polymers mentioned above, we combined acetylene-based polymer chemistry (i.e., covalent bond) and TPY-based supramolecular chemistry (non-covalent interaction) into a hybrid system to construct metallo-helicoid (**H**) with double rimmed structure. As shown in Scheme 1, a tetratopic monomer (**M**) was designed with two terminal alkynes in the outer rim for polymerization, and two terminal terpyridines (TPYs) in the inner rim for subsequent intramolecular coordination-driven self-assembly. Because of the different length of two rims, intramolecular coordination played a more predominant role in folding the metal-free polymer (**P**) to form energy-favorable secondary structure with helicoidal conformation compared to intermolecular coordination. We envisioned that **H** might be able to interact with DNA molecule through electrostatic interactions between positive charged tubular cavity and phosphate anions of DNA molecule. As such, the helicity of **H** may be induced by DNA to achieve controlled helical orientation. Moreover, tetraphenylethylene (TPE) as an iconic aggregation-induced emission (AIE) fluorophore was incorporated into the backbone of **H**.[11] The coordination of ⟨TPY-Zn(II)-TPY⟩ as well as the encapsulation of DNA resulted in restricted intramolecular motions (RIMs) of TPE, and thus leading to the enhancement of fluorescent intensity.[12]

Results and Discussion

Synthesis and Characterization of Metallo-helicoid (H)

Tetratopic monomer **M** was synthesized with two TPY units and terminal alkyne groups in the inner and outer rim of TPE core, respectively through several steps of Suzuki and Sonogashira cross-coupling reactions in decent yields as outlined in Schemes S1–2. To increase the solubility and balance the hydrophobicity/hydrophilicity of **M**, two triethylene glycol (TEG) chains were modified onto the periphery. The intermediate precursors and **M** were fully characterized by nuclear magnetic resonance (NMR), including ^{1}H, ^{13}C, Two-Dimensional Correlation Spectroscopy (2D-COSY), Nuclear Overhauser Effect Spectroscopy (2D-NOESY), high resolution Electrospray Ionization-Time of Flight (ESI-TOF) and Matrix-Assisted Laser Desorption/Ionization-Time of Flight (MALDI-TOF) mass spectrometers. The covalent polymer (**P**) was prepared by polymerization of **M** through efficient Glaser-Hay homocoupling in an O_2 atmosphere (Scheme S3).[13] Gel permeation chromatography (GPC) analyses gave a number average molecular weight (M_n) of 36 k Da and a polydispersity index (PDI) of 1.95 for **P** (Figure S37). In the MALDI-TOF mass spectrum of **P** (Figure 2), a series of peaks with a specific interval approximate 1525 Da could be observed, corresponding to the molecular weight of a repeating unit. For example, a high molecular weight signal up to ca. 53 375 Da was observed with the degree of polymerization of 35, indicating the successful synthesis of corresponding metal-free polymers. It is worth noting that MALDI-TOF generally displays an asymmetrical distribution of peaks for polymers with higher abundant signals at low m/z range due to the high ionization efficiency of oligomers with low molecular weight.[14]

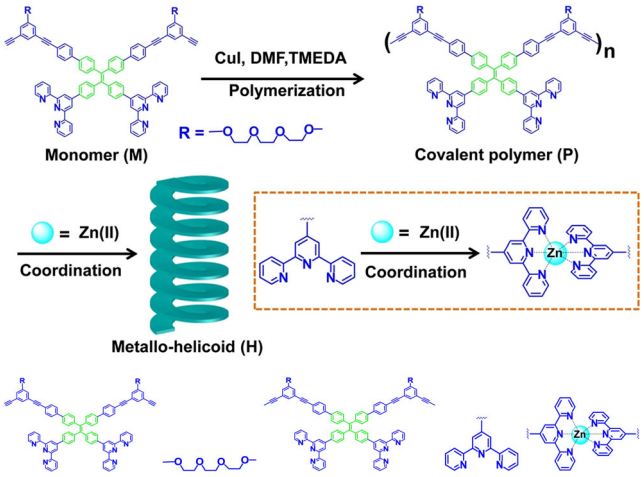

Scheme 1. The preparation of metallo-helicoid (**H**) by polymerization and folding via intramolecular coordination-driven self-assembly successively. The linear covalent polymer (**P**) was folded by Zn(II) to give rise to **H**.

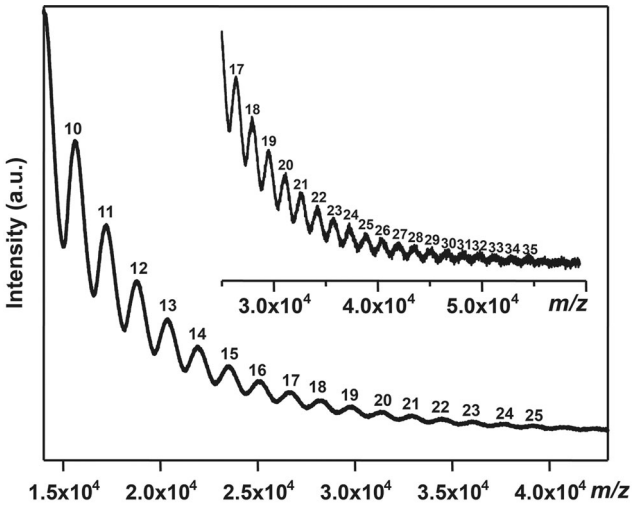

Figure 2. MALDI-TOF mass spectrum of **P** with corresponding number of repeating units. Inset: higher molecular weight region.

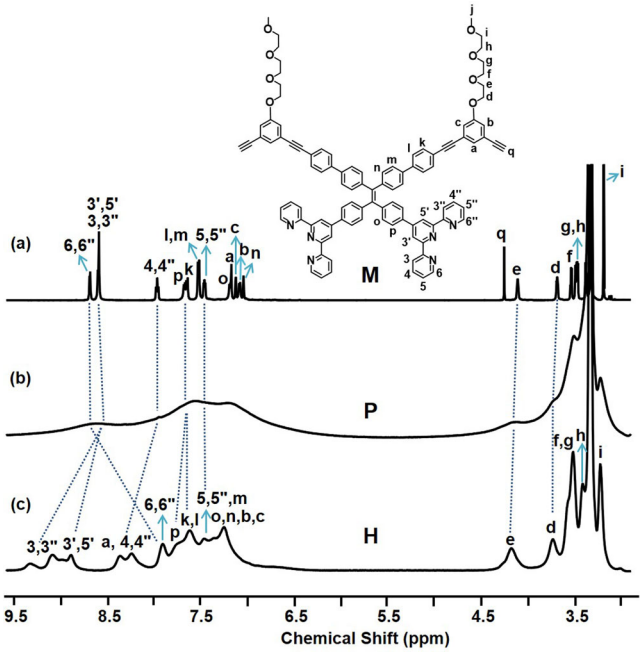

Figure 3. [1]H-NMR spectra of a) monomer **M**, b) covalent polymer **P** and c) metallo-helicoid **H** (600 MHz, 300 K, *[D$_6$]DMSO*).

Compared with the sharp [1]H NMR of **M** (Figure 3a), the spectrum of **P** (Figure 3b) showed broad signals with many overlapping in both aromatic and aliphatic region. This is attributed to the rigid π-conjugated TPE-containing polymers with high polymerization degree and multiple conformations.[15] Metallo-helicoid **H** was prepared by adding Zn-$(NO_3)_2{\cdot}6H_2O$ (0.5 equiv of TPY units) into a DMSO solution of **P** at 80 °C under vigorous stirring for 12 h. Upon adding Zn(II), several peaks of **H** (Figure 3c) in aromatic region were shifted downfield compared with **P** due to TPY-Zn(II) coordination.[16] For instance, signals of 3′, 3″ and 4′, 4″ of **H** were shifted toward the downfield by ca. 0.5 ppm compared with corresponding signals of **M** and **P**. On the contrary, the signals of the outer rim such as ^{b}H, ^{c}H, ^{k}H and ^{l}H were slightly shifted to downfield. Similarly, the peaks of ^{o}H and ^{p}H in the inner rim of **H** showed minor shift as a result of both shielding effect from the helical conformation and losing electron density by coordination. In contrast, the [1]H NMR of **H** displayed sharper signals than **P**, indicating the presence of ordered conformation with relatively immobilized skeleton. Besides, as shown in Ultraviolet-visible (UV-vis) absorption spectra (Figure S47), an obvious hypochromic effect[8e,17] was observed with respect to the formation of **H**. Such reduced UV absorbance further confirmed the successful preparation of corresponding **H**.

From the modeling structures (Figure 4), we reasoned that the large dimension of this polymer system could facilitate further structural characterization by transmission electron microscopy (TEM), atomic force microscopy (AFM), scanning tunneling microscopy (STM) and small angle X-ray scattering (SAXS) experiments. Indeed, in TEM imaging of **P**, plenty of nano-fibers with a uniform diameter (ca. 5 nm) were observed on Cu grid, which is probably attributed to the self-assembly of **P** with both rigid hydrophobic moieties (i.e., TPE and TPY) and hydrophilic TEG (Figures 5 and S38).[18] AFM imaging of **P** was consistent with TEM results, showing fiber-like nanostructures on freshly cleaved highly oriented pyrolytic graphite (HOPG) surfaces (Figures 6a–c and S40). The formation of **H** was first evidenced by TEM. Compared with **P**, the TEM images of **H** exhibited jagged surface morphologies with larger size. The images revealed uniform rod-like structures with a diameter ca. 7 nm (Figures 5d–f and S39), which is in good agreement with modeling structure without TEG (Figure 4B) on account of the low contrast of TEG in TEM imaging. This result demonstrated that **H** was successfully formed as the energy-favorable structure by means of

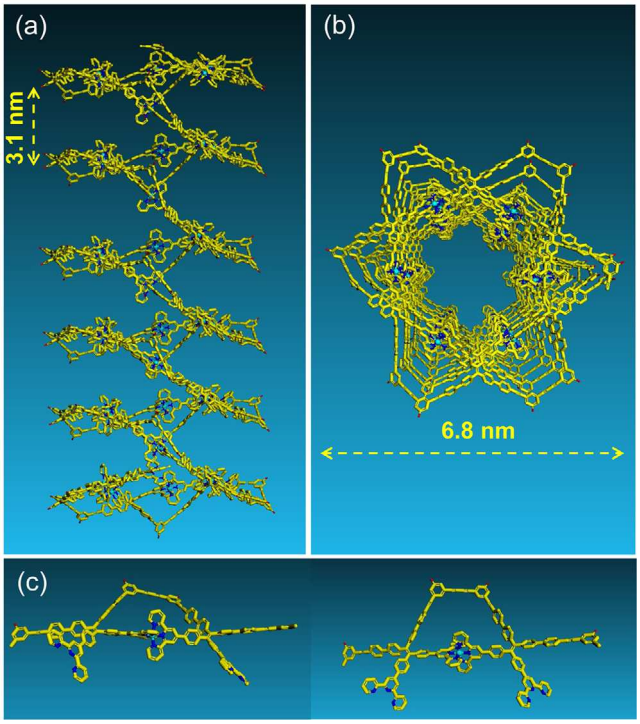

Figure 4. Energy-minimized structures of **H** with 36 repeating units, a) side-view, b) top-view, and c) basic unit. TEG chains were omitted

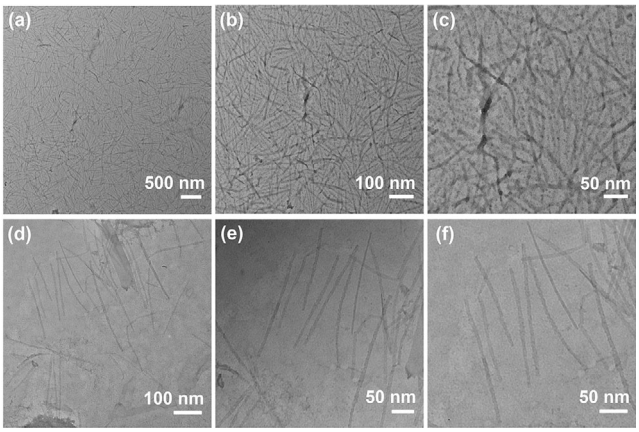

Figure 5. TEM images of (a–c) metal-free polymer (**P**) and (d–f) metallo-helicoid (**H**).

intramolecular coordination-driven self-assembly as we designed. However, the handedness of **H** is indistinguishable due to its narrow pitch and low resolution in TEM.

To further investigate the structure of **H**, we performed AFM experiments on HOPG substrates. As shown in Figures 6d–f and S41, the images exhibited helical rod-like structures with comparable measured diameter ca. 10 nm (Figures 5d–f). The value of the diameter was slightly bigger than that obtained from TEM results and molecular simulation (Figure 4) due to the insufficient resolution and unavoidable tip broadening effect of AFM.[19] As such, the observed helical pitch of **H** by AFM was around 10.5 nm, which could be a sum of multiple real pitches (Figure S43). Both right- and left-handed **H** (racemic helical structures) existed equally on HOPG owing to the same probability of helical wrapping of **P** during intramolecular coordination-driven self-assembly.

Encapsulation of DNA by H

Considering the positively charged inner rims of **H**, we reasoned that **H** might be able to interact with negatively charged DNA molecules through electrostatic interactions.[20] Interestingly, in the presence of double strand DNA (dsDNA) molecules (Figures 6g–i and S42), the length of **H** was further elongated. We speculated that DNA molecules could bridge several metallo-helicoids together. In the case of **H** binding with dsDNA, the helical nanorod was further extended up to tens of micrometres. Remarkably, only right-handed complexes (**H** ⊃ dsDNA) could be observed. This result implies that the right-handed dsDNA could induce the chiral conversion of host **H** to give rise to preferred right-handed conformation. It was also found that the angle between the crest and main axis of **H** was decreased from ca. 40° to 10° after binding with dsDNA due to multiple electrostatic interactions.

With enhanced resolution, STM could provide more accurate structural information of supramolecules.[7d,21] In order to gain more insights into the structural characterization, STM experiments were conducted for **H** and its complexes with DNA. As revealed in Figures 6d–f and S41, both right- and left-handed **H** with relatively uniform diameter were observed on the HOPG surface, agreeing well with TEM imaging. Similarly, as shown in the Figures 7a–c and S44, both right- and left-handed of **H** with a diameter ca. 7 nm in average can be observed. On the contrary, in terms of **H** ⊃ dsDNA, only right-handed **H** can be detected as exhibited in the Figures 7d–f and S45. This result further proved that the helicity of **H** could be successfully induced by

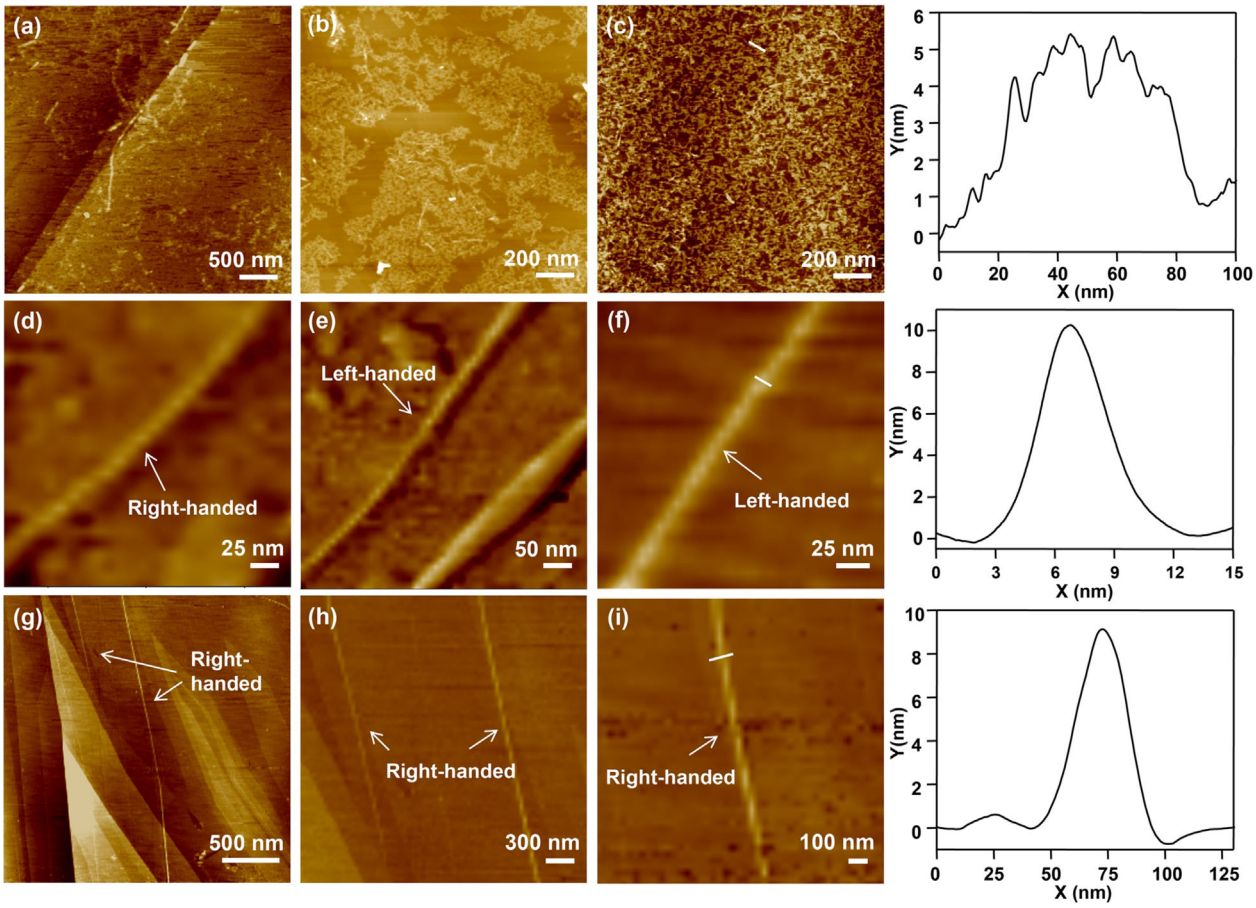

Figure 6. AFM images of metal-free polymer (**P**), metallo-helicoid (**H**) and its complex with dsDNA. AFM images of (a–c) **P**, (d–f) **H**, and (g–i) **H** ⊃ dsDNA. The cross-sectional profiles (rightmost) are along the white lines, including **P** (top), **H** (middle), and **H** ⊃ dsDNA (bottom).

dsDNA. From the height of section analysis, dsDNA could be encapsulated in the cavity of **H** (Figures 7d,e).[22]

Saturation Transfer Difference (Decay)-NMR Spectroscopy (STD-NMR) experiment was also performed on the **H** ⊃ dsDNA complex to examine if the dsDNA was encapsulated into the **H**.[23] As displayed in the Figure S33, an internal hydrogen signal (peak 6,6″) at 7.91 ppm derived from the **H** was saturated while an off-resonance reference was pulsed at 11.00 ppm. STD difference was clearly observed for dsDNA signals, indicating the interactions between dsDNA and internal cavity of **H**. The Diffusion-Ordered NMR Spectroscopy (DOSY-NMR) experiments on free dsDNA and the complex of **H** ⊃ dsDNA further confirmed this interaction. The decay rate of dsDNA was decreased after binding with **H** as revealed in the Figure S34, implying that the larger hydrodynamic radius of **H** ⊃ dsDNA complex compared with free dsDNA.

Absorbance Property of H and Its Complexes with DNA

Circular dichroism (CD) spectroscopy was further utilized to validate the chirality of helical polymers.[24] In terms of **H**, the Cotton effect was absent in DMSO solution (Figure 8a), indicating the existence of enantiomeric helical conformations of **H**. On the contrary, the complex of **H** and dsDNA (**H**

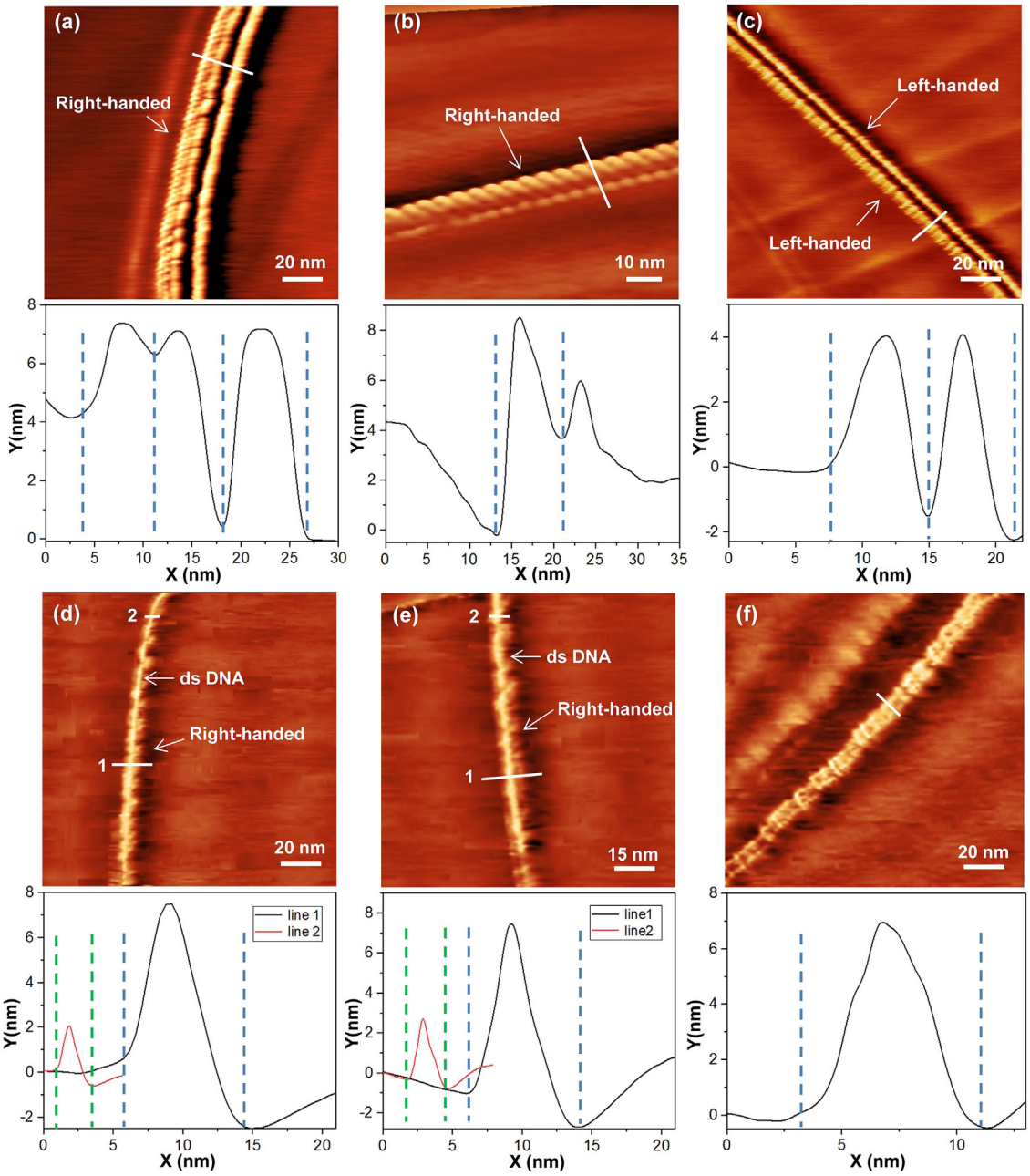

Figure 7. STM images of **H** and its complex with dsDNA. STM images of (a–c) **H**, and (d–f) **H** ⊃ dsDNA. STM line profiling measurements (bottom) are performed along the white lines for **H** and complexes, and red lines for dsDNA.

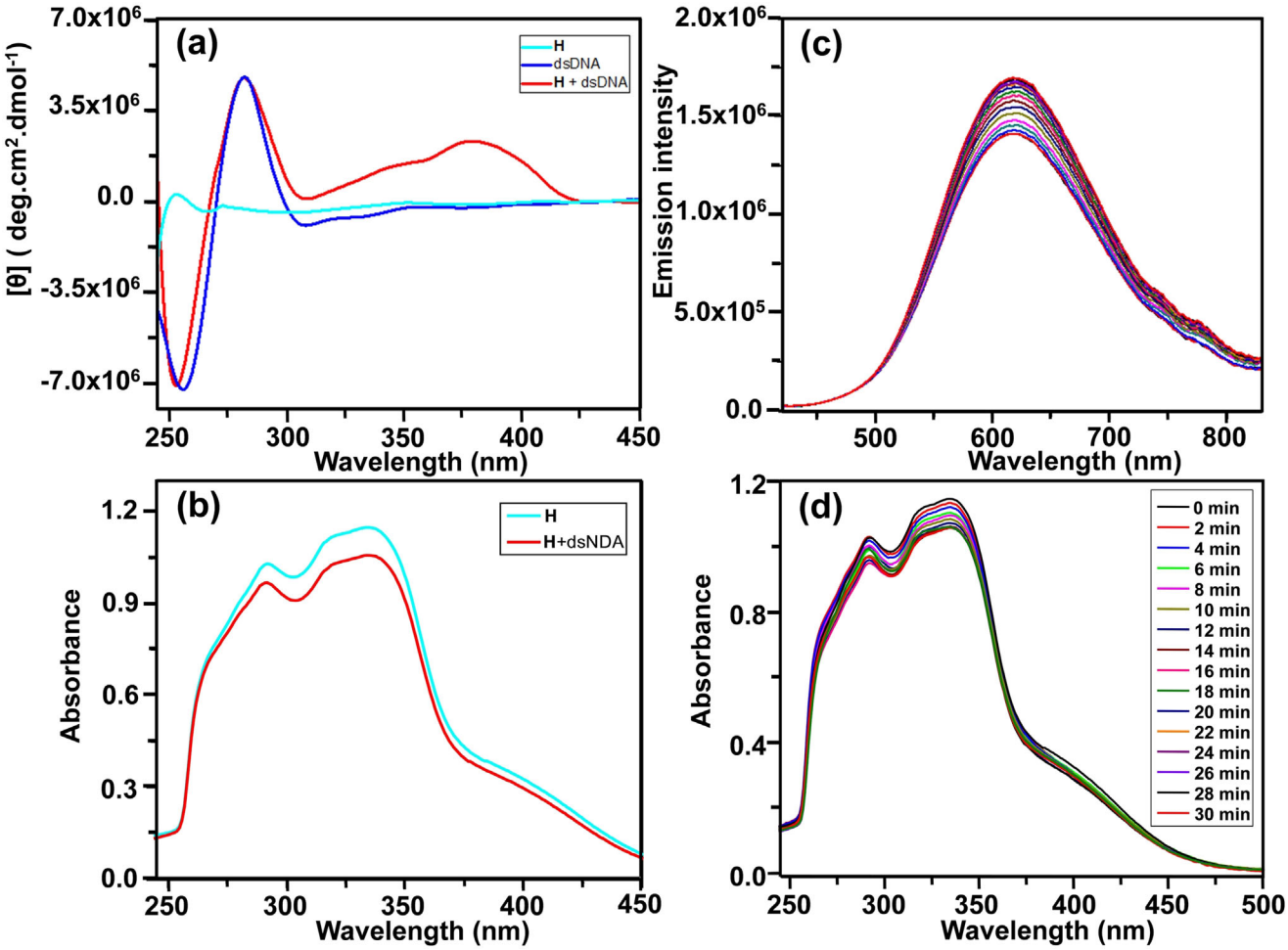

Figure 8. a) Chiral induction: CD spectra of dsDNA, **H**, and **H** ⊃ dsDNA, b) UV absorbance of **H** and **H** ⊃ dsDNA. The concentrations of dsDNA and **H** are 1.2 μM, 12 μM in DMSO, respectively. c) Time-dependent fluorescence spectra (λ_{ex} = 325 nm), d) UV absorbance of **H** ⊃ dsDNA, the concentration of dsDNA and **H** are 0.01 μM, and 12 μM in DMSO, respectively.

⊃ dsDNA) showed characteristic induced CD signals in the vicinity of 375 nm, indicating that the chirality was transferred from right-handed dsDNA to the host **H**. Meanwhile, the CD spectrum of dsDNA exhibited a positive band at around 280 nm and a negative band at ca. 250 nm, which are characteristic signals of a right-handed B conformation. This result implied the integrity of the chiral structure of dsDNA during the complexation with **H**. Furthermore, UV-vis absorbance of the complex (**H** ⊃ dsDNA) was reduced compared with **H** originating from the hypochromic effect (Figure 8b). Such results suggested that dsDNA could stabilize the helical conformation of **H** with the aid of multiple electrostatic interactions.

Emission and RIM effects

Time-dependent fluorescence spectroscopy was carried out to monitor the process of DNA encapsulation. It is anticipated that the compact helical **H** and its complex with DNA would emit intensively in solution state on account of RIM by coordination and complexation (Figures S46). The maximum emission peak of **H** is located at ca. 610 nm in DMSO solution. In addition, the binding of DNA led to the enhancement of emission intensity because of further immobilization of TPE fluorophore. Indeed, as shown in Figure 8c, upon the addition of DNA, the solution exhibited consecutive increments of emission intensity until reaching equilibrium (ca. 20 minutes). It was attributed to the introduction of additional RIM via multiple electrostatic interactions. As revealed in Figure 8c, the emission peak of the complex of **H** and dsDNA centered in ca. 610 nm. Notably, the emission intensity of **H** showed a constant increase from 1.40×10^6 to 1.75×10^6 with the addition of dsDNA. In addition, the time-dependent UV-vis absorption spectra further evidenced the encapsulation of dsDNA molecule (Figure 8d). The absorbance was decreased until reaching equilibrium along with time due to the further stabilization of **H** by electrostatic interactions. Also, we performed control experiments where DNA molecules were mixed with metal-free polymer (**P**). As displayed in the Figures S48, the emission intensity of the mixtures almost remained constant in the duration of the incubation.

SAXS Study of H and Its Complexes with dsDNA

The SAXS data of **H** and **H** ⊃ dsDNA provide important insights into the transformation of achiral **H** to chiral **H** ⊃ dsDNA. Due to the nature of SAXS, the interpreted structure should be representative of the whole sample. Figure 9 shows the SAXS data of **H** and **H** ⊃ dsDNA in DMSO. The fact that the SAXS data of **H** can be well described by a core–shell cylindrical (CSC) model with a Gaussian peak agrees with the morphology from TEM images. The best fitting shell thickness and inner radius are (0.7 ± 0.2) and (4.7 ± 0.1) nm, respectively, with a length of the cylinder >100 nm (beyond the SAXS probing range), yielding an outer diameter of 10.8 nm. The inclusion of the Gaussian peak at $q=0.2$ Å^{-1} is required in order to fit the SAXS data in the higher q regime better and the peak position corresponds to a well-defined distance, $D=2\pi/q\approx3.1$, consistent with the pitch distance from the molecular modeling (Figure 4a) as well. The SAXS data of **H** ⊃ dsDNA, as compared with that of pristine **H**, reveal distinct differences. First, steeper intensity decay was found in the low q region, causing deviation from the CSC model, while the scattering feature at medium- and high- q regime is similar to that of **H**. Here, we applied a combinational scattering model of power law decay, CSC and a broad Gaussian peak. The best fitting power law decay yields $q^{-3.5}$, corresponding to the surface scattering from large aggregates. Most intriguingly, the best fit using CSC model yields a smaller inner radius of (4.0 ± 0.04) nm but similar shell thickness of (0.7 ± 0.1) nm and slightly larger pitch distance of 3.5 nm compared to **H** tube. The original best-fitting CSC for helicoid **H** does not agree well with the SAXS data of **H** ⊃ dsDNA (Figure S50), confirming the reduction of coil radius.

The fact that the increased pitch distance (≈13%) corresponds to the reduced helicoidal diameter (≈13%) well implies possible stretching of the **H** after interaction with the dsDNA. We hypothesize that electron-negative dsDNA is likely driven into the coil by the electrostatic attraction in the presence of electron-positive chelated Zn(II) sites which are presumably located at the vicinity of the inner wall of the polymer coil. As a result, the entrapped dsDNA slightly modulates the pitch spacing of **H** from 3.1 nm to 3.5 nm and slightly reduces the inner diameter of the **H** coil. It should be noted that the diameter of dsDNA is much smaller than the inner diameter of the coil and therefore such entrapment would not significantly reduce the total entropy of the system. The short-range interaction between dsDNA and **H** is expected to introduce chirality of the dsDNA to the system as shown in Figure 8a. The fact that the shell thickness remains the same (even in the presence of dsDNA) suggests that the induction of molecular chirality does not require large quantities of dsDNA to be at presence.

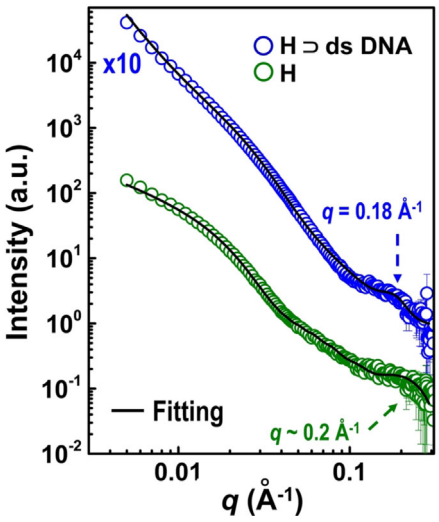

Figure 9. The 1D SAXS patterns of **H** and **H** ⊃ dsDNA. The solid lines are the best fits for the two data sets. Rescaling factors are applied to the **H** with dsDNA for better visual clarity.

Conclusion

In summary, we constructed a novel type of spiral polymer, namely, metallo-helicoid through the combination of conventional polymerization and coordination-driven self-assembly. This hybrid strategy allowed us to harness the stability of covalent polymers and the dynamic nature of non-covalent interactions into one system. More importantly, the conformation of helicoids could be precisely folded through intramolecular coordination on the basis of the double-rimmed design. The so-formed spiral structure with large cavity and high density of positive charge was able to accommodate dsDNA as the guest molecule. Remarkably, the helicity of the helicoid could be induced by the right-handedness of dsDNA. The success of this study inspired us to explore a strategy to regulate the formation of helicoidal metallo-polymers with specific handedness but without using chiral inducing agents for ongoing study.

Acknowledgements

The authors acknowledge the support from Shenzhen University and University of South Florida. X.L. also acknowledges the support from Tencent Founders Alumni Foundation.

Conflict of interest

The authors declare no conflict of interest.

Keywords: coordination-driven self-assembly · helicoid · metallo-polymers · terpyridine · tetraphenylethylene

[1] a) K. Aratsu, R. Takeya, B. R. Pauw, M. J. Hollamby, Y. Kitamoto, N. Shimizu, H. Takagi, R. Haruki, S. I. Adachi, S. Yagai, *Nat. Commun.* **2020**, *11*, 1623; b) A. Rafiei Miandashti, L. Khosravi Khorashad, M. E. Kordesch, A. O. Govorov, H. H. Richardson, *ACS Nano* **2020**, *14*, 4188–4195.
[2] D. R. Smyth, *Development* **2016**, *143*, 3272–3282.
[3] a) K. R. MacKenzie, *Chem. Rev.* **2006**, *106*, 1931–1977; b) R. O. J. Weinzierl, *Chem. Rev.* **2013**, *113*, 8350–8376.

[4] a) C. Piguet, M. Borkovec, J. Hamacek, K. Zeckert, *Coord. Chem. Rev.* **2005**, *249*, 705 – 726; b) Y. Takezawa, M. Shionoya, *Acc. Chem. Res.* **2012**, *45*, 2066 – 2076; c) M. Boiocchi, L. Fabbrizzi, *Chem. Soc. Rev.* **2014**, *43*, 1835 – 1847; d) M. Albrecht, *Chem. Rev.* **2001**, *101*, 3457 – 3498; e) M. Ikeda, Y. Tanaka, T. Hasegawa, Y. Furusho, E. Yashima, *J. Am. Chem. Soc.* **2006**, *128*, 6806 – 6807; f) V. E. Campbell, X. de Hatten, N. Delsuc, B. Kauffmann, I. Huc, J. R. Nitschke, *Nat. Chem.* **2010**, *2*, 684 – 687.

[5] a) D.-W. Zhang, X. Zhao, J.-L. Hou, Z.-T. Li, *Chem. Rev.* **2012**, *112*, 5271 – 5316; b) Y. Tanaka, H. Katagiri, Y. Furusho, E. Yashima, *Angew. Chem. Int. Ed.* **2005**, *44*, 3867 – 3870; *Angew. Chem.* **2005**, *117*, 3935 – 3938; c) H. Ito, Y. Furusho, T. Hasegawa, E. Yashima, *J. Am. Chem. Soc.* **2008**, *130*, 14008 – 14015; d) T. Maeda, Y. Furusho, S.-I. Sakurai, J. Kumaki, K. Okoshi, E. Yashima, *J. Am. Chem. Soc.* **2008**, *130*, 7938 – 7945; e) V. Berl, I. Huc, R. G. Khoury, M. J. Krische, J.-M. Lehn, *Nature* **2000**, *407*, 720 – 723; f) S. A. Denisov, Q. Gan, X. Wang, L. Scarpantonio, Y. Ferrand, B. Kauffmann, G. Jonusauskas, I. Huc, N. D. McClenaghan, *Angew. Chem. Int. Ed.* **2016**, *55*, 1328 – 1333; *Angew. Chem.* **2016**, *128*, 1350 – 1355; g) K. Ziach, C. Chollet, V. Parissi, P. Prabhakaran, M. Marchivie, V. Corvaglia, P. P. Bose, K. Laxmi-Reddy, F. Godde, J.-M. Schmitter, S. Chaignepain, P. Pourquier, I. Huc, *Nat. Chem.* **2018**, *10*, 511 – 518; h) B. Gong, *Acc. Chem. Res.* **2008**, *41*, 1376 – 1386; i) L. Yuan, H. Zeng, K. Yamato, A. R. Sanford, W. Feng, H. S. Atreya, D. K. Sukumaran, T. Szyperski, B. Gong, *J. Am. Chem. Soc.* **2004**, *126*, 16528 – 16537; j) M. Inouye, M. Waki, H. Abe, *J. Am. Chem. Soc.* **2004**, *126*, 2022 – 2027; k) A. Suzuki, K. Aratsu, S. Datta, N. Shimizu, H. Takagi, R. Haruki, S. I. Adachi, M. Hollamby, F. Silly, S. Yagai, *J. Am. Chem. Soc.* **2019**, *141*, 13196 – 13202; l) R. Misra, S. Dey, R. M. Reja, H. N. Gopi, *Angew. Chem. Int. Ed.* **2018**, *57*, 1057 – 1061; *Angew. Chem.* **2018**, *130*, 1069 – 1073; m) J.-L. Hou, X.-B. Shao, G.-J. Chen, Y.-X. Zhou, X.-K. Jiang, Z.-T. Li, *J. Am. Chem. Soc.* **2004**, *126*, 12386 – 12394.

[6] H. Yamada, Z.-Q. Wu, Y. Furusho, E. Yashima, *J. Am. Chem. Soc.* **2012**, *134*, 9506 – 9520.

[7] a) A. J. Varni, A. Fortney, M. A. Baker, J. C. Worch, Y. Qiu, D. Yaron, S. Bernhard, K. J. T. Noonan, T. Kowalewski, *J. Am. Chem. Soc.* **2019**, *141*, 8858 – 8867; b) H. Goto, Y. Furusho, K. Miwa, E. Yashima, *J. Am. Chem. Soc.* **2009**, *131*, 4710 – 4719; c) Y.-C. Zhang, L. Chen, H. Wang, Y.-M. Zhou, D.-W. Zhang, Z.-T. Li, *Chin. Chem. Lett.* **2016**, *27*, 817 – 821; d) J. Zhu, Z. Dong, S. Lei, L. Cao, B. Yang, W. Li, Y. Zhang, J. Liu, J. Shen, *Angew. Chem. Int. Ed.* **2015**, *54*, 3097 – 3101; *Angew. Chem.* **2015**, *127*, 3140 – 3144; e) Q. Gan, C. Bao, B. Kauffmann, A. Grélard, J. Xiang, S. Liu, I. Huc, H. Jiang, *Angew. Chem. Int. Ed.* **2008**, *47*, 1715 – 1718; *Angew. Chem.* **2008**, *120*, 1739 – 1742.

[8] a) H. Juwarker, J.-m. Suk, K.-S. Jeong, *Chem. Soc. Rev.* **2009**, *38*, 3316 – 3325; b) T. Nakano, Y. Okamoto, *Chem. Rev.* **2001**, *101*, 4013 – 4038; c) E. Yashima, K. Maeda, Y. Furusho, *Acc. Chem. Res.* **2008**, *41*, 1166 – 1180; d) E. Yashima, K. Maeda, H. Iida, Y. Furusho, K. Nagai, *Chem. Rev.* **2009**, *109*, 6102 – 6211; e) J. C. Nelson, J. G. Saven, J. S. Moore, P. G. Wolynes, *Science* **1997**, *277*, 1793 – 1796; f) M. Toya, H. Ito, K. Itami, *Tetrahedron Lett.* **2018**, *59*, 1531 – 1547; g) E. Yashima, N. Ousaka, D. Taura, K. Shimomura, T. Ikai, K. Maeda, *Chem. Rev.* **2016**, *116*, 13752 – 13990.

[9] a) Z. Zheng, L. Opilik, F. Schiffmann, W. Liu, G. Bergamini, P. Ceroni, L.-T. Lee, A. Schütz, J. Sakamoto, R. Zenobi, J. VandeVondele, A. D. Schlüter, *J. Am. Chem. Soc.* **2014**, *136*, 6103 – 6110; b) S. Bode, L. Zedler, F. H. Schacher, B. Dietzek, M. Schmitt, J. Popp, M. D. Hager, U. S. Schubert, *Adv. Mater.* **2013**, *25*, 1634 – 1638; c) F. Schlütter, A. Wild, A. Winter, M. D. Hager, A. Baumgaertel, C. Friebe, U. S. Schubert, *Macromolecules* **2010**, *43*, 2759 – 2771; d) U. S. Schubert, C. Eschbaumer, *Angew. Chem. Int. Ed.* **2002**, *41*, 2892 – 2926; *Angew. Chem.* **2002**, *114*, 3016 – 3050; e) A. Winter, U. S. Schubert, *Chem. Soc. Rev.* **2016**, *45*, 5311 – 5357; f) H. Hofmeier, U. S. Schubert, *Chem. Soc. Rev.* **2004**, *33*, 373 – 399; g) Z. Li, Y. Li, Y. Zhao, H. Wang, Y. Zhang, B. Song, X. Li, S. Lu, X.-Q. Hao, S.-W. Hla, Y. Tu, X. Li, *J. Am. Chem. Soc.* **2020**, *142*, 6196 – 6205; h) Z. Zhang, Y. Li, B. Song, Y. Zhang, X. Jiang, M. Wang, R. Tumbleson, C. Liu, P. Wang, X.-Q. Hao, T. Rojas, A. T. Ngo, J. L. Sessler, G. R. Newkome, S. W. Hla, X. Li, *Nat. Chem.* **2020**, *12*, 468 – 474.

[10] a) R. Dobrawa, F. Würthner, *J. Polym. Sci. Part A* **2005**, *43*, 4981 – 4995; b) Z. Li, J. Gu, S. Qi, D. Wu, L. Gao, Z. Chen, J. Guo, X. Li, Y. Wang, X. Yang, Y. Tu, *J. Am. Chem. Soc.* **2017**, *139*, 14364 – 14367; c) A. Fermi, G. Bergamini, M. Roy, M. Gingras, P. Ceroni, *J. Am. Chem. Soc.* **2014**, *136*, 6395 – 6400; d) P. Chen, Q. Li, S. Grindy, N. Holten-Andersen, *J. Am. Chem. Soc.* **2015**, *137*, 11590 – 11593; e) Y.-J. He, T.-H. Tu, M.-K. Su, C.-W. Yang, K. V. Kong, Y.-T. Chan, *J. Am. Chem. Soc.* **2017**, *139*, 4218 – 4224; f) H. Maeda, R. Sakamoto, H. Nishihara, *Coord. Chem. Rev.* **2017**, *346*, 139 – 149; g) K. Zhang, Y. Zha, B. Peng, Y. Chen, G. N. Tew, *J. Am. Chem. Soc.* **2013**, *135*, 15994 – 15997.

[11] a) X. Yan, T. R. Cook, P. Wang, F. Huang, P. J. Stang, *Nat. Chem.* **2015**, *7*, 342 – 348; b) X. Yan, M. Wang, T. R. Cook, M. Zhang, M. L. Saha, Z. Zhou, X. Li, F. Huang, P. J. Stang, *J. Am. Chem. Soc.* **2016**, *138*, 4580 – 4588; c) L.-J. Chen, Y.-Y. Ren, N.-W. Wu, B. Sun, J.-Q. Ma, L. Zhang, H. Tan, M. Liu, X. Li, H.-B. Yang, *J. Am. Chem. Soc.* **2015**, *137*, 11725 – 11735.

[12] a) Z. Zhao, H. Zhang, J. W. Y. Lam, B. Z. Tang, *Angew. Chem. Int. Ed.* **2020**, *59*, 9888 – 9907; *Angew. Chem.* **2020**, *132*, 9972 – 9993; b) R. T. K. Kwok, C. W. T. Leung, J. W. Y. Lam, B. Z. Tang, *Chem. Soc. Rev.* **2015**, *44*, 4228 – 4238; c) J. Mei, N. L. C. Leung, R. T. K. Kwok, J. W. Y. Lam, B. Z. Tang, *Chem. Rev.* **2015**, *115*, 11718 – 11940; d) R. Hu, N. L. C. Leung, B. Z. Tang, *Chem. Soc. Rev.* **2014**, *43*, 4494 – 4562; e) G.-Q. Yin, H. Wang, X.-Q. Wang, B. Song, L.-J. Chen, L. Wang, X.-Q. Hao, H.-B. Yang, X. Li, *Nat. Commun.* **2018**, *9*, 567.

[13] a) S. Chaudhuri, M. Mohanan, A. V. Willems, J. A. Bertke, N. Gavvalapalli, *Chem. Sci.* **2019**, *10*, 5976 – 5982; b) B. B. Ahuja, A. Vigalok, *Angew. Chem. Int. Ed.* **2019**, *58*, 2774 – 2778; *Angew. Chem.* **2019**, *131*, 2800 – 2804.

[14] G. Montaudo, F. Samperi, M. S. Montaudo, *Prog. Polym. Sci.* **2006**, *31*, 277 – 357.

[15] a) R. Hu, R. Ye, J. W. Y. Lam, M. Li, C. W. T. Leung, B. Zhong Tang, *Chem. Asian J.* **2013**, *8*, 2436 – 2445; b) Q. Chen, J.-X. Wang, F. Yang, D. Zhou, N. Bian, X.-J. Zhang, C.-G. Yan, B.-H. Han, *J. Mater. Chem.* **2011**, *21*, 13554 – 13560.

[16] a) M. Wang, C. Wang, X.-Q. Hao, J. Liu, X. Li, C. Xu, A. Lopez, L. Sun, M.-P. Song, H.-B. Yang, X. Li, *J. Am. Chem. Soc.* **2014**, *136*, 6664 – 6671; b) M. Wang, K. Wang, C. Wang, M. Huang, X.-Q. Hao, M.-Z. Shen, G.-Q. Shi, Z. Zhang, B. Song, A. Cisneros, M.-P. Song, B. Xu, X. Li, *J. Am. Chem. Soc.* **2016**, *138*, 9258 – 9268.

[17] a) H.-G. Jeon, J. Y. Jung, P. Kang, M.-G. Choi, K.-S. Jeong, *J. Am. Chem. Soc.* **2016**, *138*, 92 – 95; b) M. Banno, T. Yamaguchi, K. Nagai, C. Kaiser, S. Hecht, E. Yashima, *J. Am. Chem. Soc.* **2012**, *134*, 8718 – 8728.

[18] a) S. Campioni, G. Carret, S. Jordens, L. Nicoud, R. Mezzenga, R. Riek, *J. Am. Chem. Soc.* **2014**, *136*, 2866 – 2875; b) Y. Kim, W. Li, S. Shin, M. Lee, *Acc. Chem. Res.* **2013**, *46*, 2888 – 2897; c) J. K. Sahoo, M. A. VandenBerg, E. E. Ruiz Bello, C. D. Nazareth, M. J. Webber, *Nanoscale* **2019**, *11*, 16534 – 16543.

[19] a) F. Taraballi, M. Campione, A. Sassella, A. Vescovi, A. Paleari, W. Hwang, F. Gelain, *Soft Matter* **2009**, *5*, 660 – 668; b) K. Jiang, L. S. Schadler, R. W. Siegel, X. Zhang, H. Zhang, M. Terrones, *J. Mater. Chem.* **2004**, *14*, 37 – 39.

[20] Y. Kim, H. Li, Y. He, X. Chen, X. Ma, M. Lee, *Nat. Nanotechnol.* **2017**, *12*, 551 – 556.

[21] a) M. C. O'Sullivan, J. K. Sprafke, D. V. Kondratuk, C. Rinfray, T. D. W. Claridge, A. Saywell, M. O. Blunt, J. N. O'Shea, P. H. Beton, M. Malfois, H. L. Anderson, *Nature* **2011**, *469*, 72 – 75;

b) D. V. Kondratuk, L. M. A. Perdigão, A. M. S. Esmail, J. N. O'Shea, P. H. Beton, H. L. Anderson, *Nat. Chem.* **2015**, *7*, 317 – 322.
[22] a) H. Tanaka, C. Hamai, T. Kanno, T. Kawai, *Surf. Sci.* **1999**, *432*, L611 – L616; b) H. Tanaka, T. Kawai, *Nat. Nanotechnol.* **2009**, *4*, 518 – 522.
[23] a) L. Ye, N. Van Eps, M. Zimmer, O. P. Ernst, R. Scott Prosser, *Nature* **2016**, *533*, 265 – 268; b) A. Viegas, J. Manso, F. L. Nobrega, E. J. Cabrita, *J. Chem. Educ.* **2011**, *88*, 990 – 994.
[24] C. C. Lee, C. Grenier, E. W. Meijer, A. P. H. J. Schenning, *Chem. Soc. Rev.* **2009**, *38*, 671 – 683.

Manuscript received: August 4, 2020
Revised manuscript received: September 14, 2020
Accepted manuscript online: October 2, 2020
Version of record online: ■■ ■■, ■■■■

Research Articles

Polymerization

G.-Q. Yin, S. Kandapal, C.-H. Liu, H. Wang, J. Huang, S.-T. Jiang, T. Ji, Y. Yan, S. Khalife, R. Zhou, L. Ye, B. Xu, H.-B. Yang, M.-P. Nieh, X. Li* _____ ▮▮▮▮–▮▮▮▮

Metallo-Helicoid with Double Rims: Polymerization Followed by Folding by Intramolecular Coordination

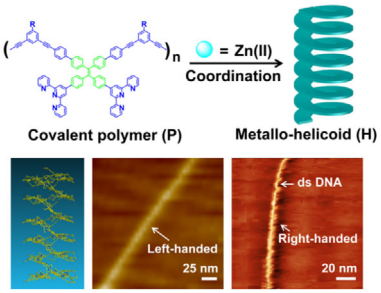

A new type of metallo-polymer with helicoidal structure was constructed through the combination of covalent polymerization and intramolecular coordination-driven self-assembly. Owing to the positive charges on the inner rim of helicoid, double-stranded DNA molecules (dsDNA) could interact with metallo-helicoid (**H**) via electrostatic interactions. Notably, dsDNA allowed exclusive formation of **H** with right handedness by means of chiral induction.